Published for SISSA by Springer

Received: May 17, 2022
Revised: July 23, 2022
Accepted: August 20, 2022
Published: September 12, 2022

A tower of hidden sectors: a general treatment and physics implications

Amin Aboubrahim[a] **and Pran Nath**[b]

[a] *Institut für Theoretische Physik, Westfälische Wilhelms-Universität Münster, Wilhelm-Klemm-Straße 9, 48149 Münster, Germany*
[b] *Department of Physics, Northeastern University, 111 Forsyth Street, Boston, MA 02115-5000, U.S.A.*

E-mail: aabouibr@uni-muenster.de, p.nath@northeastern.edu

Abstract: An analysis of a tower of hidden sectors coupled to each other, with one of these hidden sectors coupled to the visible sector, is given and the implications of such couplings on physics in the visible sector are investigated. Thus the analysis considers n number of hidden sectors where the visible sector couples only to hidden sector 1, while the latter couples also to hidden sector 2, and the hidden sector 2 couples to hidden sector 3 and so on. A set of successively feeble couplings of the hidden sectors to the visible sector are generated in such a set up. In general each of these sectors live in a different heat bath. We develop a closed form set of coupled Boltzmann equations for the correlated evolution of the temperatures and number densities of each of the heat baths. We then apply the formalism to a simplified model with scalar portals between the different sectors. Predictions related to dark matter direct detection experiments and future CMB probes of dark radiation are made.

Keywords: Particle Nature of Dark Matter, Cosmology of Theories BSM, Models for Dark Matter

ArXiv ePrint: 2205.07316

https://doi.org/10.1007/JHEP09(2022)084

JHEP09(2022)084

Contents

JHEP09(2022)084

1 Introduction

Most modern theories of particle physics based on supergravity, strings and branes contain hidden sectors which are neutral under the Standard Model (SM) gauge group but may possess their own gauge groups. However, even though the hidden sectors are neutral under the SM gauge group, they may possess feeble interactions with the visible sector via a variety of portals such as the Higgs portal, kinetic and Stueckelberg mass mixings between the hidden sector U(1) gauge fields and the visible sector $\mathrm{U}(1)_Y$ hypercharge gauge field, or via higher dimensional operators which are dually charged under the gauge groups of the Standard Model and of the hidden sectors. The visible and the hidden sectors will in general reside in different heat baths. In prior literature, it is often assumed (see, e.g. [1, 2]) that the visible and the hidden sectors temperature evolution are governed by entropy conservation carried out separately for the visible and the hidden sectors. However, such an assumption is untenable if there is a coupling between the hidden sectors and the visible sector. Thus

a proper treatment of the temperatures of the visible and the hidden sectors implies that one perform their evolution consistent with conservation of the total entropy and not the entropy conservation for each sector separately. An analysis of such a formalism was given in ref. [3] for the case of one hidden sector and for the case of two hidden sectors in ref. [4]. Further, an application of ref. [3] was made for the explanation of EDGES anomaly [5] in ref. [6] (for related works see [7–10]). It is to be noted that the extension to two hidden sectors brings in new physics. Thus with one hidden sector, it is not possible to have dark photon as dark matter because it is not possible to satisfy the twin constraints that the dark photon simultaneously have a lifetime larger than the lifetime of the universe and at the same give us significant amount of dark matter consistent with the Planck data [11]. We expect that further extensions of the formalism involving more hidden sectors would also bring in new physics which may have implications for particle physics and cosmology.

Thus in this work we extend the analysis to the case of n number of hidden sectors which are linked to the visible sector in a sequential manner. Specifically, if we label the visible and the hidden sectors as $S_a, a = 0, 1, \cdots, n$ where S_0 stands for the visible sector and $S_a, a = 1, \cdots, n$ stand for the hidden sectors, then we assume that the sectors have only next neighbor couplings. That is to say that a sector S_i has couplings only with S_{i-1} and S_{i+1}. In this setup, we investigate the correlated evolution of temperatures in each sector relative to a given reference temperature. While such a reference temperature can be chosen arbitrarily, in this analysis we assume the temperature of the visible sector to be the reference temperature or the 'clock'. Specifically, we obtain a set of n coupled Boltzmann equations for the temperature evolution functions $\xi_a = T_a/T, a = 1, 2, \cdots, n$, where T is the temperature of the visible sector and T_a $(a = 1, \cdots, n)$ is the temperature of hidden sector a. An analysis is also given of how very feeble couplings can be obtained by a sequential couplings of the hidden sectors to the visible sector. For some early works related to the evolution of hidden and visible sectors see, e.g., [12, 13].

The outline of the rest of the paper is as follows: in section 2, we discuss the model with n hidden sectors, and in section 3 we apply this generalization to n hidden sectors to the Stueckelberg extension of the SM. In section 4 we discuss the special case of three hidden sectors for a simple model consisting of a dark Dirac fermion and dark scalar particles. In section 5 we study the thermal effect of hidden sectors on experimentally measured observables such as the spin-independent proton-DM scattering cross-section and on dark radiation given by $\Delta N_{\rm eff}$ for extra light relics. Conclusions are given in section 6. A detailed derivation of the evolution equations for visible and hidden sector temperatures is given in appendix A and the collision and source terms used in the Boltzmann equations are listed in appendix B.

2 A model with n hidden sectors

The model consists of n number of hidden sectors linked in a chain with the first hidden sector connected to the visible sector as shown in figure 1.

The above is a generalization of the cases considered previously for $n = 1$ and $n = 2$. As mentioned earlier, we choose the temperature of the visible sector as the clock. The set

JHEP09(2022)084

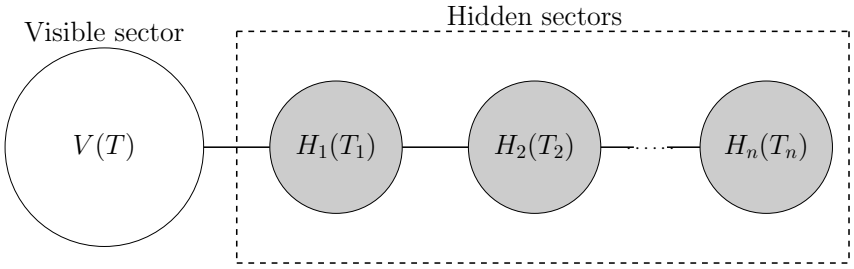

Figure 1. The visible sector linked to a chain of n number of hidden sectors.

of Boltzmann equations for the energy density ρ_α including energy exchange between the sectors is $d\rho_\alpha/dt + 3H(p_\alpha + \rho_\alpha) = j_\alpha$ $(\alpha = 0, 1, 2, \cdots, n)$. For the range of masses for the dark sector particles we consider in this analysis, it is safe to assume radiation domination[1] down to $T \sim 10^{-5}\,\text{GeV}$ and so $p_\alpha = 1/3\rho_\alpha$. Thus, we get

$$\frac{d\rho_\alpha}{dt} + 4H\rho_\alpha = j_\alpha, \qquad \alpha = 0, 1, 2, \ldots, n\,, \tag{2.1}$$

where $\alpha = 0$ refers to the visible sector and where j_α encodes in it all the possible processes exchanging energy between neighboring sectors. As discussed above, in order to properly describe the thermal evolution of the universe with visible and hidden sectors in different heat baths, we need to have evolution equations for the $d\xi_\alpha/dT$. However, to compute $d\xi_\alpha/dT, \alpha = 1, 2, \cdots, n$ we first derive equations for $d\rho_\alpha/dT$ $(\alpha = 1 \cdots n)$ in terms of $d\rho_v/dT$. We proceed by considering the Boltzmann equation of the total energy density ρ, i.e., $d\rho/dt + 4H\rho = 0$. Knowing that $d\rho/dt = (d\rho/dT)(dT/dt)$, we have

$$\frac{dT}{dt} = -\frac{4H\rho}{d\rho/dT}. \tag{2.2}$$

Next we look at the Boltzmann equations for the individual energy densities $d\rho_\alpha/dt + 4H\rho_\alpha = j_\alpha$ which after using eq. (2.2) will immediately give us

$$\frac{d\rho_\alpha}{dT} = \frac{(4H\rho_\alpha - j_\alpha)}{4H\rho}\frac{d\rho}{dT}. \tag{2.3}$$

Next we define

$$\begin{aligned} \sigma_v &= \rho - \rho_v, \\ \sigma_\alpha &= \rho - \rho_\alpha = \rho_v + \sum_{\beta\neq\alpha} \rho_\beta \quad (\alpha, \beta = 1 \cdots n), \end{aligned} \tag{2.4}$$

where the total energy density is

$$\rho = \rho_v + \sum_{\alpha=1}^{n} \rho_\alpha\,. \tag{2.5}$$

[1]Early matter domination is possible, e.g., in the presence of heavy long-lived particles and rapidly oscillating fields (such as the inflaton field). In string theory, oscillating moduli fields displaced from the minimum of their potential can dominate the energy density in the early universe. None of these situations are relevant in our analysis. The light spectrum of our dark species justify the radiation domination assumption.

JHEP09(2022)084

To reduce clutter, we define $K_\alpha \equiv (4H\rho_\alpha - j_\alpha)/4H\rho$ and so eq. (2.3) becomes

$$\frac{d\rho_\alpha}{dT} = K_\alpha \frac{d\rho}{dT} = K_\alpha \left(\frac{d\rho_v}{dT} + \frac{d\rho_\alpha}{dT} + \sum_{\beta \neq \alpha} \frac{d\rho_\beta}{dT} \right). \tag{2.6}$$

Rearranging, we get

$$\frac{d\rho_\alpha}{dT} - C_\alpha \sum_{\beta \neq \alpha} \frac{d\rho_\beta}{dT} = C_\alpha \frac{d\rho_v}{dT}, \tag{2.7}$$

where we have defined

$$C_\alpha \equiv \frac{K_\alpha}{1 - K_\alpha} = \frac{4H\rho_\alpha - j_\alpha}{4H\rho - 4H\rho_\alpha + j_\alpha} = \frac{4H\rho_\alpha - j_\alpha}{4H\sigma_\alpha + j_\alpha}. \tag{2.8}$$

Further, we may write out the coupled equation for $d\rho_\alpha/dT$ as follows

$$\begin{aligned}
&d\rho_1/dT - C_1 d\rho_2/dT - C_1 d\rho_3/dT \cdots - C_1 d\rho_n/dT = C_1 d\rho_v/dT, \\
&- C_2 d\rho_1/dT + d\rho_2/dT - C_2 d\rho_3/dT \cdots - C_2 d\rho_n/dT = C_2 d\rho_v/dT, \\
&\cdots\cdots \\
&- C_n d\rho_1/dT - C_n d\rho_2/dT - C_n d\rho_3/dT \cdots + d\rho_n/dT = C_n d\rho_v/dT.
\end{aligned} \tag{2.9}$$

We can write this in a matrix form so that

$$\begin{pmatrix}
1 & -C_1 & -C_1 & \cdots & -C_1 & -C_1 \\
-C_2 & 1 & -C_2 & \cdots & -C_2 & -C_2 \\
-C_3 & -C_3 & 1 & \cdots & -C_3 & -C_3 \\
\cdots & \cdots & \cdots & \cdots & \cdots & \cdots \\
-C_{n-1} & -C_{n-1} & -C_{n-1} & \cdots & 1 & -C_{n-1} \\
-C_n & -C_n & -C_n & \cdots & -C_n & 1
\end{pmatrix}
\begin{pmatrix}
d\rho_1/dT \\ d\rho_2/dT \\ d\rho_3/dT \\ \cdots \\ d\rho_{n-1}/dT \\ d\rho_n/dT
\end{pmatrix}
=
\begin{pmatrix}
C_1 \\ C_2 \\ C_3 \\ \cdots \\ C_{n-1} \\ C_n
\end{pmatrix} d\rho_v/dT. \tag{2.10}$$

This equation can be written in a compact form so that

$$\sum_{\beta=1}^{n} \mathcal{C}_{\alpha\beta} \frac{d\rho_\beta}{dT} = C_\alpha \frac{d\rho_v}{dT}, \tag{2.11}$$

where the matrix $\mathcal{C}$ is the square matrix on the left hand side of eq. (2.10). Thus $d\rho_\alpha/dT$ can be written as

$$\frac{d\rho_\alpha}{dT} = \sum_{j=1}^{n} \left(\mathcal{C}^{-1}\right)_{\alpha\beta} C_\beta \frac{d\rho_v}{dT}. \tag{2.12}$$

Note that one may also write

$$\rho'_\alpha = \frac{d\rho_\alpha}{dT} = P_\alpha + Q_\alpha \xi'_\alpha, \qquad \alpha = 1, 2, \cdots, n-1, n, \tag{2.13}$$

where $\xi'_\alpha \equiv d\xi_\alpha/dT$ and where P_α and Q_α are defined so that

$$P_\alpha = \xi_\alpha \frac{dP_\alpha}{dT_\alpha}, \qquad Q_\alpha = T \frac{d\rho_\alpha}{dT_\alpha}. \tag{2.14}$$

JHEP09(2022)084

Thus we have an equation for $d\xi_\alpha/dT$ which takes the form

$$\frac{d\xi_\alpha}{dT} = -\frac{P_\alpha}{Q_\alpha} + \sum_{\beta=1}^{n} \left(C^{-1}\right)_{\alpha\beta} C_\beta \frac{\rho_v'}{Q_\alpha}, \qquad \alpha = 1, 2, \cdots, n-1, n. \tag{2.15}$$

Eqs. (2.15) give us n differential equations for the evolution functions $d\xi_\alpha/dT$. These have to be solved along with the Boltzmann equations governing the number density evolution of the hidden sector particles. This will allow us to determine the relic densities of all stable species and describe the thermal evolution of this coupled system.

For the special case of three hidden sectors, the matrix $\mathcal{C}$ is given by

$$\mathcal{C} = \begin{pmatrix} 1 & -C_1 & -C_1 \\ -C_2 & 1 & -C_2 \\ -C_3 & -C_3 & 1 \end{pmatrix}. \tag{2.16}$$

Therefore we can write eq. (2.12) in a matrix form so that

$$\begin{pmatrix} d\rho_1/dT \\ d\rho_2/dT \\ d\rho_3/dT \end{pmatrix} = \frac{1}{D} \begin{pmatrix} (1-C_2C_3) & C_1(1+C_3) & C_1(1+C_2) \\ C_2(1+C_3) & (1-C_1C_3) & C_2(1+C_1) \\ C_3(1+C_2) & C_3(1+C_1) & (1-C_1C_2) \end{pmatrix} \begin{pmatrix} C_1 \\ C_2 \\ C_3 \end{pmatrix} d\rho_v/dT, \tag{2.17}$$

where D is given by

$$D = 1 - C_1C_2 - C_1C_3 - C_2C_3 - 2C_1C_2C_3. \tag{2.18}$$

Since $\rho_\alpha' = P_\alpha + Q_\alpha \xi_\alpha'$, we have

$$\xi_\alpha' \equiv \frac{d\xi_\alpha}{dT} = -\frac{P_\alpha}{Q_\alpha} + \frac{1}{Q_\alpha}\rho_\alpha'. \tag{2.19}$$

Therefore the individual expressions can be easily obtained as

$$\frac{d\xi_1}{dT} = -\frac{P_1}{Q_1} + \frac{1}{Q_1 D}\left[C_1 + C_1C_2 + C_1C_3 + C_1C_2C_3)\right] d\rho_v/dT, \tag{2.20}$$

$$\frac{d\xi_2}{dT} = -\frac{P_2}{Q_2} + \frac{1}{Q_2 D}\left[C_2 + C_1C_2 + C_2C_3 + C_1C_2C_3)\right] d\rho_v/dT, \tag{2.21}$$

$$\frac{d\xi_3}{dT} = -\frac{P_3}{Q_3} + \frac{1}{Q_3 D}\left[C_3 + C_2C_3 + C_1C_3 + C_1C_2C_3)\right] d\rho_v/dT. \tag{2.22}$$

These equations give the evolution of the temperature ratios $\xi_\alpha = T_\alpha/T, \alpha = 1, 2, 3$.

Before proceeding further, we note here that a chain of n hidden sectors analogous to the one of figure 1 appears in well known scenarios of physics beyond the Standard Model such as in moose/quiver gauge theories (see, e.g., [14–17]). Thus an analysis of the type above may find application in a broader class of particle physics models beyond the Standard Model.

JHEP09(2022)084

3 Theory application: the Stueckelberg extension of the standard model

The Stueckelberg extension of the SM with an extra hidden $\mathrm{U}(1)_X$ gauge group offers the possibility of a hidden sector feebly coupled to the visible sector. The gauged $\mathrm{U}(1)_X$ gives rise to a dark photon which, under certain conditions, can be a dark matter candidate [4, 18]. In this section we give the analytic expressions for a Stueckelberg extension of the SM to n hidden sectors which the above formalism can easily be applied to.

3.1 Generation of very feeble couplings from kinetic mixings via a chain of hidden sectors

As discussed in section 2, we consider the following type of couplings: the visible sector couples to the hidden sector 1 (H_1), the hidden sector 1 couples to hidden sector 2 (H_2) and so on, up to hidden sector $(n-1)$ which couples to the hidden sector n (H_n). The couplings between the sectors could be via kinetic mixing [19], via Stueckelberg mass mixing [20], via both kinetic mixing and Stueckelberg mass mixing [21] and contain matter in the hidden sectors [20, 22] (for recent works based on Stueckelberg extensions of the Standard Model see also [23, 24]). Specifically we assume that each of the n number of hidden sectors possess a $\mathrm{U}(1)_{X_I}$ gauge invariance with a gauge field $A_I^\mu, I = 1, \cdots, n$. Including the gauge field B_μ for the hypercharge $\mathrm{U}(1)_Y$, we have $n+1$ U(1) gauge fields which we collectively denote by $V_i^\mu, i = 1, \cdots, n+1$ where we define the elements of V_i as follows:

$$(V) = (V_1 = B, V_2 = A_1, \cdots, V_{n+1} = A_n), \tag{3.1}$$

where B_μ is the hypercharge field of the visible sector and $A_{I\mu},\ I = 1, \cdots, n$ are the gauge fields for the hidden sector $\mathrm{U}(1)_{X_I},\ I = 1, \cdots, n$. We assume the gauge fields have kinetic mixings and Stueckelberg mass mixings and such mixings to be sequential and thus the Lagrangian for the gauge fields is assumed to be of the form

$$\begin{aligned}\mathcal{L}_{\mathrm{km}} = &-\frac{1}{4}\left[\sum_{i=1}^{n+1} G_{i\mu\nu}G_i^{\mu\nu} + 2\sum_{i=1}^{n}\delta_i G_{i\mu\nu}G_{i+1}^{\mu\nu}\right] \\ &-\frac{1}{2}\sum_{i=1}^{n}(M_i V_{i\mu} + \mu_i V_{i+1\mu} + \partial_\mu\sigma_i)^2.\end{aligned} \tag{3.2}$$

Note that there are n axion fields $\sigma_i,\ i = 1, \cdots, n$ which are absorbed by the n gauge fields of the hidden sectors to become massive.

We note that the fields in the Lagrangian above are not in their canonical form. Further, this Lagrangian must be coupled with the Standard Model Higgs field in the electroweak symmetry breaking. After the electroweak symmetry breaking, one must make the appropriate transformations to put the Lagrangian in the canonical form. We give now a brief discussion of this procedure. In the analysis below we will include the third component of the gauge fields for $\mathrm{SU}(2)_L(\mathcal{A}_3)$ of the SM since that fields along with the hypercharge gauge field enter in giving mass to the W and Z bosons in the electroweak symmetry breaking. The transformation that puts the kinetic energy in the canonical form is given by

$$\mathcal{V}_\mu = K\mathcal{V}'_\mu\,, \tag{3.3}$$

JHEP09(2022)084

where our notation is the following[2]

$$\mathcal{V}_\mu^T = (\{\mathcal{V}_a\}) = (\mathcal{A}_{3\mu}, V_{1\mu}, V_{2\mu}, V_{3\mu}, \cdots, V_{n\mu}, V_{n+1,\mu}), a = 0, \cdots, n+1,$$
$$\mathcal{V}_\mu^{\prime T} = (\{\mathcal{V}'_a\}) = (\mathcal{A}_{3\mu}, V'_{1\mu}, V'_{2\mu}, V'_{3\mu}, \cdots, V'_{n\mu}, V'_{n+1,\mu}), a = 0, \cdots, n+1,$$

and where K is an $(n+2)\times(n+2)$ dimensional matrix defined as

$$K = \begin{pmatrix} 1 & 0 & 0 & 0 & 0 & \cdot & \cdot & 0 \\ 0 & 1 & -s_1 & s_1 s_2 & -s_1 s_2 s_3 & \cdot & \cdot & (-1)^n s_1 s_2 \cdots s_n \\ 0 & 0 & c_1 & -c_1 s_2 & c_1 s_2 s_3 & \cdot & \cdot & (-1)^{(n-1)} c_1 s_2 \cdots s_n \\ 0 & 0 & 0 & c_2 & -c_2 s_3 & \cdot & \cdot & (-1)^{(n-2)} c_2 s_3 \cdots s_n \\ \cdot & \cdot & \cdot & \cdot & \cdot & \cdot & \cdot & \cdot \\ 0 & 0 & 0 & 0 & 0 & 0 & c_{(n-1)} & -c_{(n-1)} s_n \\ 0 & 0 & 0 & 0 & 0 & 0 & 0 & c_n \end{pmatrix}, \tag{3.4}$$

where in general c_k and s_k (for $k = 1, \ldots, n$) are given by

$$c_k = \frac{\sqrt{1 - \sum_{i=1}^{k-1} \delta_i^2}}{\sqrt{1 - \sum_{i=1}^{k} \delta_i^2}}, \quad s_k = \frac{\delta_k}{\sqrt{1 - \sum_{i=1}^{k} \delta_i^2}}. \tag{3.5}$$

Note that c_k, s_k satisfy the relation $c_k^2 - s_k^2 = 1$. In the transformed coordinates the kinetic energy part of the Lagrangian takes the form $\mathcal{L} = -\frac{1}{4}\mathcal{V}'^T_{\mu\nu}\mathcal{V}'^{\mu\nu}$. Next, we focus on the mass terms. In addition to the Stueckelberg mass terms involving the visible and the hidden sectors, we have mass terms for $A_0, \mathcal{A}_3$ from the Higgs mechanism which have the form

$$\mathcal{L}^m_{\rm SM} = -\frac{1}{2}\left(\frac{1}{4} g_Y^2 v^2 B^\mu B_\mu + \frac{1}{4} g_2^2 v^2 \mathcal{A}_3^\mu \mathcal{A}_{3\mu} + \frac{1}{2} g_1 g_2 v^2 B^\mu \mathcal{A}_3^\mu\right), \tag{3.6}$$

where $v = (\sqrt{2} G_F)^{-1/2}$ and where G_F is the Fermi constant. Thus we write the total mass term for the gauge fields so that

$$\mathcal{L}_m = -\frac{1}{2}\mathcal{V}_\mu^T M^2 \mathcal{V}^\mu, \tag{3.7}$$

where M^2 includes the mass terms both from the Higgs mechanism and from the Stueckelberg mass growth mechanism. After the transformation that diagonalizes the kinetic energy, the mass term is given by

$$\mathcal{L}_m = -\frac{1}{2}\mathcal{V}'^T_\mu M'^2 \mathcal{V}'^\mu, \tag{3.8}$$

where $\mathcal{V}'^\mu$ is defined in eq. (3.3) and $M'^2 = K^T M^2 K$. Since M'^2 is a symmetric matrix it can be diagonalized by an orthogonal transformation R so that $R^T R = I$. Thus the transformation $\mathcal{V}' = R\mathcal{E}$, or $\mathcal{V} = KR\mathcal{E}$ diagonalizes the mass matrix.

$$M_D^2 = \mathcal{O}^T M^2 \mathcal{O},$$
$$\mathcal{V} = \mathcal{O}\mathcal{E}, \tag{3.9}$$

[2]Note that while $V_{i\mu}$ has i taking values $i = 1, \ldots, n+1$, $\mathcal{V}_a$ has a taking values $a = 0, 1, \cdots, n+1$.

JHEP09(2022)084

where $\mathcal{O} = KR$ and both the kinetic and the mass terms are in a canonically diagonal basis and we have

$$\mathcal{L} = -\frac{1}{4}\mathcal{E}^T_{\mu\nu}\mathcal{E}^{\mu\nu} - \frac{1}{2}\mathcal{E}^T_{\mu} M_D^2 \mathcal{E}^{\mu}. \tag{3.10}$$

We note that the subcase $n = 2$ was discussed in [25]. We arrange the vector mass eigenstates $\mathcal{E}_\mu$ so that $\mathcal{E}^T = (Z, A_\gamma, A_{\gamma_2}, \ldots, A_{\gamma_3}, \cdots, A_{\gamma_n})$. Thus the mass eigenstates consist of the Z boson, the photon, and n number of dark photons in the hidden sector.

3.2 Neutral currents of the coupled visible and hidden sectors

Since the mixings involve the neutral gauge bosons of the visible and the hidden sectors, we begin by displaying the interactions of these gauge bosons in their respective sectors. Thus the neutral current interactions of the visible and the hidden sectors together are

$$\mathcal{L}_{\rm NC} = g_2 J_2^\mu \mathcal{A}_{3\mu} + g_Y J_Y^\mu B_\mu + \sum_{i=1}^{n} g_{Xi} J_{Xi}^\mu A_{i\mu}. \tag{3.11}$$

In the equation above, matter charged under a hidden sector gauge field $A_{i\mu}$ will reside in the source term J^μ_{Xi}. Such matter may consist of dark fermions and dark complex scalar fields charged under the $\mathrm{U}(1)_{Xi}$. Thus if we have Dirac fermions D_{Xi} charged under $\mathrm{U}(1)_{Xi}$ we will have $J^\mu_{Xi} = \bar{D}_{Xi}\gamma^\mu D_{Xi}$.

To write the neutral currents in a compact notation in the $\mathcal{V}$ basis, we define

$$\begin{aligned}
&(\mathcal{V}_a): \quad (\mathcal{A}_{3\mu}, B_\mu, A_{1\mu}, \cdots, A_{n\mu}),\\
&(\mathcal{G}_a): \quad \mathcal{G}_0 = g_2, \quad \mathcal{G}_1 = g_Y, \quad \mathcal{G}_3 = g_{X_1}, \cdots, \quad \mathcal{G}_{n+1} = g_{X_n} \quad a = 0, \cdots, n+1,\\
&(\mathcal{J}_a): \quad \mathcal{J}_0^\mu = J_2^\mu, \quad \mathcal{J}_1^\mu = J_Y^\mu, \cdots, \quad \mathcal{J}_{i+1}^\mu = J_{X_i}^\mu, \quad a = 0, \cdots, n+1\\
&(\mathcal{E}_a): \quad \mathcal{E}_0^\mu = Z^\mu, \quad \mathcal{E}_1^\mu = A_\gamma^\mu, \quad \mathcal{E}_2^\mu = A_{\gamma_2}^\mu, \cdots,, \quad \mathcal{E}_{n+1}^\mu = A_{\tilde{\gamma}_n}^\mu, \quad a = 0, \cdots, n+1,
\end{aligned} \tag{3.12}$$

where Z^μ is the Z-boson field, A^μ_γ is the photon field, and $A^\mu_{\tilde{\gamma}_i}, \cdots, A^\mu_{\tilde{\gamma}_n}$ are the fields for the dark photons. We now rewrite the neutral current interaction so that

$$\mathcal{L}_{\rm NC} = \sum_{a=0}^{n+1} \mathcal{G}_a \mathcal{J}_a^\mu \mathcal{V}_a. \tag{3.13}$$

Next we write $\mathcal{L}_{\rm NC}$ in terms of the mass eigenstates $\mathcal{E}$ so that

$$\mathcal{L}_{\rm NC} = \sum_{a=0}^{n+1} \mathcal{G}_a \mathcal{J}_a^\mu \mathcal{O}_{ab} \mathcal{E}_{b\mu}. \tag{3.14}$$

We can now display the coupling of the Z boson and the photon and for the dark photon in an explicit manner. Thus we can decompose the couplings into several parts so that

$$\mathcal{L}_{\rm NC} = \mathcal{L}^{\rm NC}_{\rm SM} + \mathcal{L}_{Z\gamma D} + \mathcal{L}_{{\rm SM}\tilde{\gamma}} + \mathcal{L}_{D\tilde{\gamma}}, \tag{3.15}$$

JHEP09(2022)084

where

$$\begin{aligned}
\mathcal{L}_{\rm SM}^{\rm NC} &= \left(g_2 J_2^\mu \mathcal{O}_{00} + g_Y J_Y^\mu \mathcal{O}_{10}\right) Z_\mu + \left(g_2 J_2^\mu \mathcal{O}_{01} + g_Y J_Y^\mu \mathcal{O}_{11}\right) A_\mu^\gamma, \\
\mathcal{L}_{Z\gamma D} &= \sum_{a=2}^{n+1} g_{Xa} J_{Xa}^\mu \mathcal{O}_{a0} Z_\mu + \sum_{a=2}^{n+1} g_{Xa} J_{Xa}^\mu \mathcal{O}_{a1} A_\mu^\gamma, \\
\mathcal{L}_{{\rm SM}\tilde{\gamma}} &= \sum_{i=1}^{n} \left(g_2 J_2^\mu \mathcal{O}_{0(i+1)} + g_Y J_Y \mathcal{O}_{1(i+1)}\right) A_\mu^{\tilde{\gamma}_i}, \\
\mathcal{L}_{D\tilde{\gamma}} &= \sum_{i,j=1}^{n} g_{X_i} J_{X_i} \mathcal{O}_{(j+1)(i+1)} A_\mu^{\tilde{\gamma}_j}.
\end{aligned} \tag{3.16}$$

Here $\mathcal{L}_{\rm SM}^{\rm NC}$ is the modified neutral current of the Standard Model, $\mathcal{L}_{Z\gamma D}$ is the coupling of the SM gauge bosons Z, A_γ with the dark sector, $\mathcal{L}_{{\rm SM}\tilde{\gamma}}$ is the coupling of the dark photons with the SM sector and $\mathcal{L}_{D\tilde{\gamma}}$ is the coupling of the dark photons with the dark sources. The various parts of the couplings of eqs. (3.16) have the following meaning. As stated $\mathcal{L}_{\rm SM}$ is the modified neutral current of the Standard Model. $\mathcal{L}_{Z\gamma D}$ and $\mathcal{L}_{{\rm SM}\tilde{\gamma}}$ enter in the freeze-in production of the hidden sector particles, $\mathcal{L}_{{\rm SM}\tilde{\gamma}}$ enters in the decay of the dark photons, and $\mathcal{L}_{D\tilde{\gamma}}$ controls freeze-out in the dark sector, while $\mathcal{L}_{Z\gamma D}$ enters in the analysis of kinetic equilibrium of the dark sources after chemical decoupling.

4 Numerical application: the visible sector coupled to three hidden sectors

4.1 A simple model

In this section we will use the general expression of eq. (2.15) to determine the temperature evolution of a chain of hidden sectors coupled to the visible sector as described by figure 1. The hidden sectors will eventually get populated by dark particle species and so the evolution of the temperature is coupled with the evolution of the particle number densities. In refs. [3, 4] the cases of one and two hidden sectors have been considered in the context of a Stueckelberg U(1) extension of the SM. Here, we add a third hidden sector but consider a simpler model to illustrate the effect of three hidden sectors on dark matter phenomenology and on cosmology. Further, we assume that particles in the different sectors communicate via a scalar portal which will become evident next.

Our set up of the matter content of the three hidden sectors is as follows: the first hidden sector has a Dirac fermion D (which serves as one of the possible dark matter candidates) and a pseudo-scalar ϕ_1 (mediator). The field ϕ_2 is a scalar while ϕ_3 is a pseudo-scalar and are not particularly associated with any specific hidden sector. The model presented below is phenomenological and its UV completion remains to be explored. The Lagrangian of the model we use for the rest of the analysis is

$$\mathcal{L} = \mathcal{L}_{\rm SM} + \Delta\mathcal{L}, \tag{4.1}$$

where $\mathcal{L}_{\rm SM}$ is the SM Lagrangian and $\Delta\mathcal{L}$ is the Lagrangian for the hidden sector including portal interactions between the visible and the hidden sectors. We note here in passing that we are considering the hidden sector to have no gauged U(1) symmetry and for that reason

JHEP09(2022)084

there is no kinetic energy for the hidden sector gauge field or its interactions included in $\Delta\mathcal{L}$ below. Thus $\Delta\mathcal{L}$ is given by

$$\begin{aligned}\Delta\mathcal{L} = &\frac{1}{2}\sum_{i=1}^{3}\left(\partial_\mu\phi_i\partial^\mu\phi_i - m_i^2\phi_i^2\right) + \bar{D}\left(i\gamma^\mu\partial_\mu - m_D\right)D \\ &- y_q\phi_1\bar{q}\gamma^5 q - y_\ell\phi_1\bar{\ell}\gamma^5\ell - y_D\phi_1\bar{D}\gamma^5 D \\ &- \frac{\kappa_1}{3}\phi_1^2\phi_2 - \frac{\kappa_2}{3}\phi_2\phi_3^2 - \frac{1}{4}\sum_{i=1}^{3}\lambda_i\phi_i^4 - \frac{1}{4}\sum_i\sum_{j>i}\lambda_{ij}\phi_i^2\phi_j^2\,, \end{aligned} \tag{4.2}$$

where the dark fermion D resides in the hidden sector 1 and couples only to the field ϕ_1 in the hidden sector 1. The fields ϕ_1 and ϕ_3 as pseudoscalars and ϕ_2 as CP-even scalar are chosen purely on phenomenological grounds which we use to illustrate the main features of the visible sector coupling to three hidden sectors. For simplicity, we assume that ϕ_1 only couples to the first generation of quarks and leptons via the Yukawa couplings y_q and y_ℓ and to the D fermions via y_D. Thus in this model, the field ϕ_1 is the portal connecting the visible and hidden sectors. Further, for simplicity, we will assume equality of the portal field coupling to the Standard Model quarks and leptons, i.e., $y_q = y_\ell = y_f$. The size of the Yukawas could be very small. Thus, for example, a higher dimensional operator such as $\frac{H^\dagger H}{\Lambda^2}\bar{q}q$ after electroweak symmetry breaking would give $y_q \sim 10^{-9}$ for $\Lambda = \mathcal{O}(10^6)\,\text{GeV}$. A string scale such as this can arise in Type IIB string theory. The quartic couplings λ_i do not play a role in the temperature and number density evolution while we assume the couplings λ_{ij} are small compared to κ_1 and κ_2.

4.2 Evolution equations

In the set up described above, only the first hidden sector possesses direct couplings to SM (the visible sector) through the Yukawa couplings y_q and y_ℓ while the second hidden sector connects to the first and to the third hidden sectors. We assume that the visible sector is held at a temperature T and the three hidden sectors at temperatures T_1, T_2 and T_3 where one prescribes the initial values of the temperatures $T_i \ll T$ $(i = 1, 2, 3)$. The Boltzmann equations for the number and total energy densities are given by

$$\frac{dn_r}{dt} + 3Hn_r = \mathcal{Q}_r\,, \tag{4.3}$$

$$\frac{d\rho}{dt} + 3H(\rho + p) = 0, \tag{4.4}$$

with $r \in \{D, \phi_1, \phi_2, \phi_3\}$. In the above, ρ is the total energy density, p is the total pressure, H is the Hubble parameter and $\mathcal{Q}_r$ are the collision terms which include all possible particle number-changing processes. They are listed in appendix B.

After defining the co-moving number density or *yield*, $Y = n/\mathbb{s}$, where $\mathbb{s}$ is the total entropy density and using eqs. (4.3) and (4.4), we write

$$\frac{dY_r}{dT} = -\mathbb{s}\frac{d\rho/dT}{4H\rho}\mathcal{Q}_r, \tag{4.5}$$

JHEP09(2022)084

where H is related to the energy density by the Friedmann equation

$$H^2 = \frac{8\pi G_N}{3}\rho. \tag{4.6}$$

One can define the individual energy and entropy densities in terms of effective number of degrees of freedom so that

$$\rho = \frac{\pi^2}{30}\left(g^v_{\rm eff}T^4 + g_{1\rm eff}T_1^4 + g_{2\rm eff}T_2^4 + g_{3\rm eff}T_3^4\right), \tag{4.7}$$

$$\mathbb{s} = \frac{2\pi^2}{45}\left(h^v_{\rm eff}T^3 + h_{1\rm eff}T_1^3 + h_{2\rm eff}T_2^3 + h_{3\rm eff}T_3^3\right). \tag{4.8}$$

We note that $g_{\rm eff}$ and $h_{\rm eff}$ of the hidden sectors are defined as integrals which depend on the mass of the relevant particle and temperature. In appendix A, we exhibit the m/T dependence of the integrals. In the above, we need to compute T_i so that $T_i = \xi_i T$. Thus we need to write out the evolution equations for ξ_i in an explicit form. In this case we have three evolution functions $\xi_1 = T_1/T, \xi_2 = T_2/T$ and $\xi_3 = T_3/T$ and using eq. (2.15) we find that they obey the following equations

$$\frac{d\xi_1}{dT} = -\frac{P_1}{Q_1} + \frac{1}{Q_1 D}\left[C_1 + C_1C_2 + C_1C_3 + C_1C_2C_3)\right] d\rho_v/dT, \tag{4.9}$$

$$\frac{d\xi_2}{dT} = -\frac{P_2}{Q_2} + \frac{1}{Q_2 D}\left[C_2 + C_1C_2 + C_2C_3 + C_1C_2C_3)\right] d\rho_v/dT, \tag{4.10}$$

$$\frac{d\xi_3}{dT} = -\frac{P_3}{Q_3} + \frac{1}{Q_3 D}\left[C_3 + C_2C_3 + C_1C_3 + C_1C_2C_3)\right] d\rho_v/dT, \tag{4.11}$$

where D is given by

$$D = 1 - C_1C_2 - C_1C_3 - C_2C_3 - 2C_1C_2C_3. \tag{4.12}$$

For the case of one hidden sector ($n = 1$), we have $C_2 = C_3 = 0$, $D = 1$ and ξ_2 and ξ_3 are absent. In this case eq. (4.9) reads

$$\frac{d\xi_1}{dT} = -\frac{P_1}{Q_1} + C_0\frac{\rho_v'}{Q_1}, \tag{4.13}$$

which agrees with the result of ref. [3]. Next we look at the $n = 2$ case (two hidden sectors). Here we set $C_3 = 0$ and $D = 1 - C_1C_2$, so that

$$\frac{d\xi_1}{dT} = -\frac{P_1}{Q_1} + \frac{C_1 + C_2C_1}{1 - C_1C_2}\frac{\rho_v'}{Q_1}. \tag{4.14}$$

Similarly we have

$$\frac{d\xi_2}{dT} = -\frac{P_2}{Q_2} + \frac{C_1C_2 + C_2}{1 - C_1C_2}\frac{\rho_v'}{Q_2}. \tag{4.15}$$

These agree with the analysis of refs. [4, 18]. We note here that C_1, C_2, C_3 are given by

$$C_1 = \frac{4H\rho_1 - j_1}{4H\sigma_1 + j_v}, \qquad C_2 = \frac{4H\rho_2 - j_2}{4H\sigma_2 + j_2}, \qquad C_3 = \frac{4H\rho_3 - j_3}{4H\sigma_3 + j_3}, \tag{4.16}$$

JHEP09(2022)084

where the source terms admit the relation $j_v + j_1 + j_2 + j_3 = 0$. The source terms j_1, j_2 and j_3 are listed in appendix B. Carrying out some further simplifications to eqs. (4.9)–(4.11), we can write them as

$$\frac{d\xi_1}{dT} = -\frac{\xi_1}{T} + \left(\frac{4H\rho_1 - j_1}{4H\rho_v + j_1 + j_2 + j_3}\right) \frac{d\rho_v/dT}{T\frac{d\rho_1}{dT_1}}, \tag{4.17}$$

$$\frac{d\xi_2}{dT} = -\frac{\xi_2}{T} + \left(\frac{4H\rho_2 - j_2}{4H\rho_v + j_1 + j_2 + j_3}\right) \frac{d\rho_v/dT}{T\frac{d\rho_2}{dT_2}}, \tag{4.18}$$

$$\frac{d\xi_3}{dT} = -\frac{\xi_3}{T} + \left(\frac{4H\rho_3 - j_3}{4H\rho_v + j_1 + j_2 + j_3}\right) \frac{d\rho_v/dT}{T\frac{d\rho_3}{dT_3}}. \tag{4.19}$$

The factor $\frac{d\rho/dT}{4H\rho}$ appearing in eq. (4.5) involves a derivative of the total energy density with respect to the visible sector temperature. We differentiate each of the energy densities with respect to T and remembering that $\xi_\alpha = \xi_\alpha(T)$, then eq. (4.5) can be cast in the form

$$\frac{dY_r}{dT} = -\frac{\mathbb{s}}{H}\left(\frac{d\rho_v/dT}{4\rho_v - j_v/H}\right)\mathcal{Q}_r\,. \tag{4.20}$$

It is to be noted from eq. (4.20) that the source term j_v now appears in the Boltzmann equations for the particle yields. The formalism given above provides us with a set of coupled Boltzmann equations in temperature and yield which need to be numerically solved to get a full description of the thermal evolution of the hidden sectors. We do this next.

4.3 Numerical analysis

In our analysis here we consider the case of self-interacting DM, where we take $m_{\phi_1}/m_D \ll 1$ which will allow us to consider the most recent results on the DM-nucleon spin-independent (SI) cross-section from PandaX-II experiment [26] as an experimental constraint. In the following we give an analysis of three type of mass hierarchies among the matter fields of the hidden sectors which are: case 1: $m_{\phi_1} > 2m_{\phi_2}$, $m_{\phi_2} = m_{\phi_3}$; case 2: $m_{\phi_2} > 2m_{\phi_1}$, $m_{\phi_2} > 2m_{\phi_3}$; case 3: $m_{\phi_2} > 2m_{\phi_1}$, $m_{\phi_3} = 0$. For each of these cases we compute the thermal evolution given by $\xi_i = T_i/T$ for the three hidden sectors, and compute the yields. Specifically the analysis indicates the fraction of the relic density of the dark matter contributed by each of the dark sectors. We discuss each of these cases in detail below.

Case 1: $m_{\phi_1} > 2m_{\phi_2}$ and $m_{\phi_2} = m_{\phi_3}$. In figure 2 we exhibit the particle yields (left panel) and the temperature ratios ξ_i (right panel) as a function of the visible sector temperature. As the temperature T drops, the hidden sectors are gradually populated by the dark particle species. The process happens sequentially where the first hidden sector gets populated first whereas the second and third hidden sectors see an increase in the yield much later. This is because the first hidden sector is the only one with direct couplings to the visible sector whereas the other two hidden sectors rely on the first hidden sector to get populated.

Further, the energy densities of the hidden sectors depend on the temperature evolution of the respective sectors. This is illustrated in the right panel of figure 2. Here we notice

JHEP09(2022)084

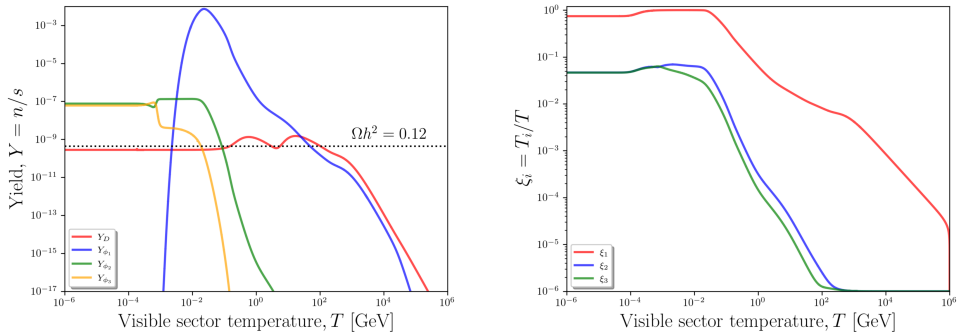

Figure 2. The case of three initially cold dark sectors. Left panel: evolution of the yields of the dark fermion D and of the spin zero particles of the dark sector versus the visible sector temperature. Right panel: evolution of the temperature ratios ξ_i. The input parameters are: $m_D = 1.0\,\text{GeV}$, $m_{\phi_1} = 50\,\text{MeV}$, $m_{\phi_2} = m_{\phi_3} = 1\,\text{MeV}$, $y_f = 1.3 \times 10^{-9}$, $y_D = 0.053$ and $\kappa_1 = \kappa_2 = 10^{-6}$. Total relic density $\Omega h^2 = 0.114$, where $\Omega h^2_D = 0.072$, $\Omega h^2_{\phi_2} = 0.0175$ and $\Omega h^2_{\phi_3} = 0.0275$. We note that the kink in ξ_i around $T = 10^{-4}\,\text{GeV}$ is due to the variation in the degrees of freedom. Specifically, this is due to neutrino decoupling and e^+e^- annihilation. Similar kinks appear in figures 4, 5 and 6.

how ξ_1 rises almost immediately starting from large T while ξ_2 and ξ_3 remain at their lowest values before picking up at $T \sim 30\,\text{GeV}$. Thus the process of thermalization begins with the first hidden sector which then permeates to the second and the third hidden sectors. However, while ξ_1 reaches 1 the other hidden sectors remain out of thermal equilibrium with $\xi_2, \xi_3 \ll 1$ and $\xi_2 \neq \xi_3$. For the benchmark considered in figure 2, the relic density is shared among D, ϕ_2 and ϕ_3 (ϕ_1 decays back to the SM particles). Note that ϕ_2 can still have a variety of off-shell decays: $\phi_2 \to \phi_1^*\phi_1^* \to \bar{q}q\bar{q}q, \ell^+\ell^-\ell^+\ell^-, \bar{q}q\ell^+\ell^-, \bar{q}q\nu\nu, \ell^+\ell^-\nu\nu, \nu\nu\nu\nu$. However, if the mass of ϕ_2 is constrained so that $m_{\phi_2} \simeq 1\,\text{MeV}$, all the decays except for the final state $\nu\nu\nu\nu$ will be forbidden. In this case the decay is extremely suppressed since $\Gamma_{\phi_2} \propto \kappa_1^2 y_f^4$,

$$\Gamma_{\phi_2} = \frac{\kappa_1^2 y_f^4}{16384\pi^5 m_{\phi_2}} \times \int_0^{m_{\phi_2}^2} dq_1^2 \int_0^{\left(m_{\phi_2}-q_1\right)^2} dq_2^2 \frac{\lambda^{1/2}\left(q_1^2, q_2^2, m_{\phi_2}^2\right) q_1^2 q_2^2}{\left[\left(q_1^2 - m_{\phi_1}^2\right)^2 + m_{\phi_1}^2\Gamma_{\phi_1}^2\right]\left[(q_2^2 - m_{\phi_1}^2)^2 + m_{\phi_1}^2\Gamma_{\phi_1}^2\right]}. \tag{4.21}$$

Thus we have $\tau_{\phi_2} \sim \mathcal{O}(10^{25})$ yrs for the input mentioned in the caption of figure 2.

As is apparent from the preceding discussion, the thermalization between the first hidden sector and the visible sector is mainly driven by the processes $\phi_1 \leftrightarrow i\,\bar{i}$, where $i\,\bar{i}$ refers to the SM particles. To illustrate this further, we plot in figure 3 the energy exchange rate for different processes as well as the energy density dilution term due to the Hubble expansion, $4H\rho_1$. In the left panel of figure 3, we consider case 1 which corresponds to the analysis of figure 2. We see that all processes are subdominant to the dilution term except

JHEP09(2022)084

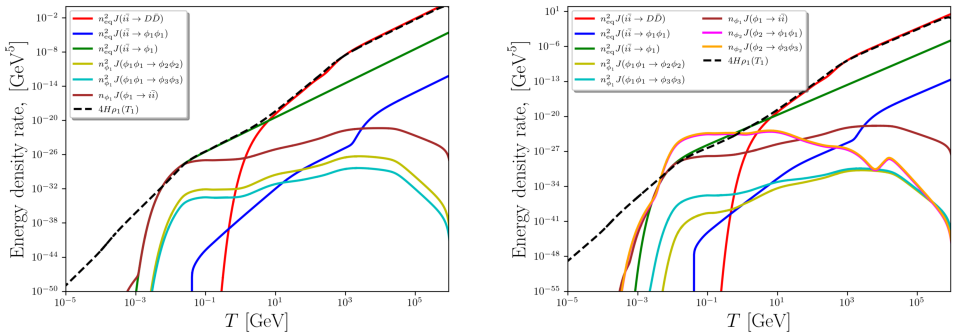

Figure 3. Plots of the energy exchange rate between different sectors versus the visible sector temperature T. The input for the left panel (Case 1) are same as in figure 2 while the input for the right panel (Case 2) are the same as in figure 5.

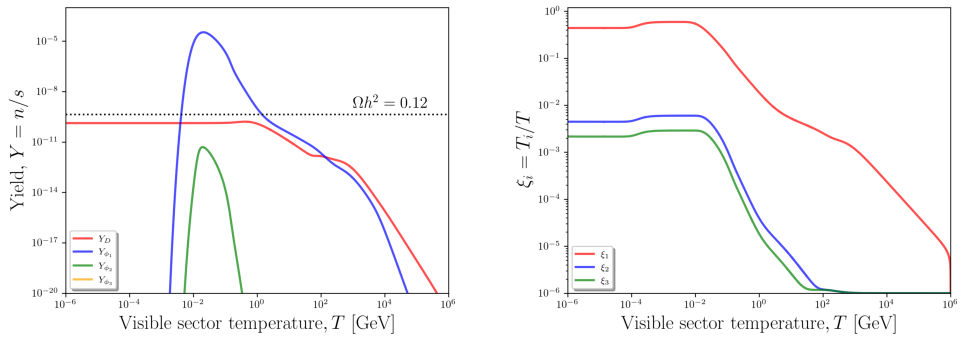

Figure 4. Same input as in figure 2 but for $y_f = 1 \times 10^{-10}$. Relic density $\Omega h^2_D = 3.6 \times 10^{-2}$ and $\Omega h^2_{\phi_2} = \Omega h^2_{\phi_3} \sim 0$.

for $i\,\bar{i} \to D\bar{D}$ and $\phi_1 \leftrightarrow i\,\bar{i}$. Of particular interest are the processes $\phi_1 \leftrightarrow i\,\bar{i}$ (green and brown curves) which become comparable in rate near 10^{-2} GeV which is the region where the two sectors thermalize as seen in the right panel of figure 2. The rates slightly overtake $4H\rho_1(T_1)$ for a short period of time before dying out due to Boltzmann suppression of the number density. The right panel of figure 3 pertains to case 2 whose discussion we leave for the next section.

Since the visible and the hidden sectors constitute a chain, a change in one coupling will propagate to all sectors. In figure 4 we consider a smaller y_f value, i.e. a weaker coupling between the visible and first hidden sector. As expected, the relic density of D becomes smaller and due to a smaller abundance of dark species in the first hidden sector, the yields of ϕ_2 and ϕ_3 become negligible (the yield of ϕ_3 does not appear in the left panel as it is extremely small). Furthermore, the first hidden sector no longer thermalizes with the visible sector as evident from the right panel of figure 4. We also note the change in the evolution of ξ_2 and ξ_3.

JHEP09(2022)084

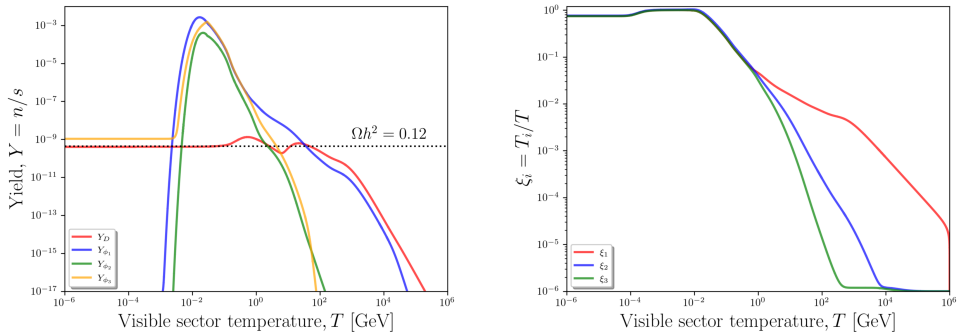

Figure 5. The case of three initially cold dark sectors. Left panel: evolution of the yields of the dark fermion D and of the spin zero particles of the dark sector versus the visible sector temperature. Right panel: evolution of the temperature ratios ξ_i. The input parameters are: $m_D = 1.0\,\text{GeV}$, $m_{\phi_1} = 50\,\text{MeV}$, $m_{\phi_2} = 105\,\text{MeV}$, $m_{\phi_3} = 45\,\text{MeV}$, $y_f = 1 \times 10^{-9}$, $y_D = 0.05$, $\kappa_1 = 10^{-7}$ and $\kappa_2 = 6 \times 10^{-6}$. Total relic density is $\Omega h^2 = 0.1198$, where $\Omega h^2_D = 0.102$ and $\Omega h^2_{\phi_3} = 0.0178$.

Case 2: $m_{\phi_2} > 2m_{\phi_1}$ and $m_{\phi_2} > 2m_{\phi_3}$. For this mass hierarchy, both decay processes $\phi_2 \to \phi_1\phi_1$ and $\phi_2 \to \phi_3\phi_3$ are kinematically allowed. We solve the coupled Boltzmann equations for this case and plot in figure 5 the yields of the dark species as well as ξ_i against the visible sector temperature.

As one would expect, ϕ_1 as well as ϕ_2 completely decay leaving D and ϕ_3 as the two possible DM components. For the benchmark considered in figure 5, the energy exchange rate due to the processes $\phi_2 \to \phi_3\phi_3$ and $\phi_2 \to \phi_1\phi_1$ are comparable and reach values larger than the energy density dilution due to the Hubble expansion (see the magenta and orange curves in the right panel of figure 3) which results in a rapid thermalization between the three hidden sectors as seen in the right panel of figure 5. Notice that all three sectors remain very much in close thermal contact while also reaching thermal equilibrium with the visible sector for a period of time.

Case 3: $m_{\phi_2} > 2m_{\phi_1}$ and $m_{\phi_3} = 0$. With the same setup as before we assume now that particle ϕ_3 is massless. The evolution of the yields of the dark particles as well as the temperature ratios ξ_i are shown in figure 6. The DM relic density is satisfied as seen from the left panel.

Even though ϕ_3 resides in the third hidden sector, the coupling y_f between the first hidden sector and the visible has an important effect on ξ_3 owing to the coupled nature of the system. Smaller values of y_f will lead to smaller ξ_3 and hence a lower contribution to ΔN_{eff}. We study this in more detail in the next section.

5 Implications for observables

In this section we discuss the physical consequences of the formalism given above. In subsection 5.1 we discuss the thermal effects of hidden sectors on the proton-DM scattering cross sections. In subsection 5.2 we discuss the contribution to dark radiation from hidden sectors.

JHEP09(2022)084

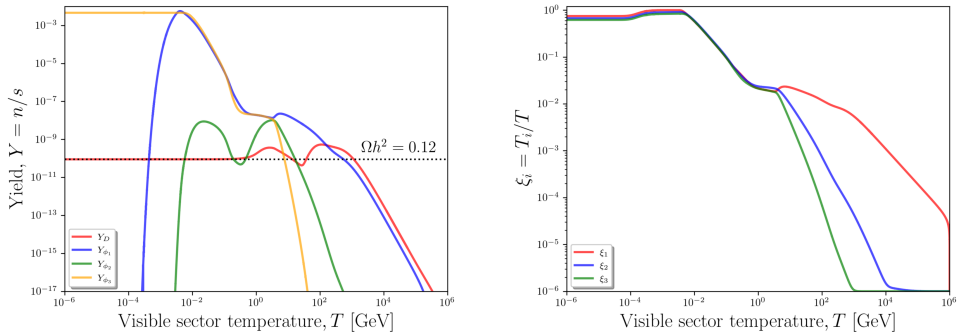

Figure 6. The case of three initially cold dark sectors. Left panel: evolution of the yields of the dark fermion D and the scalars of the dark sector versus the visible sector temperature. Right panel: evolution of the temperature ratios ξ_i. The input parameters are: $m_D = 5.0\,\text{GeV}$, $m_{\phi_1} = 10\,\text{MeV}$, $m_{\phi_2} = 105\,\text{MeV}$, $m_{\phi_3} = 0$, $y_f = 6.7 \times 10^{-10}$, $y_D = 0.17$ and $\kappa_1 = \kappa_2 = 10^{-7}$. Total relic density is $\Omega h^2 = \Omega h_D^2 = 0.123$. As discussed in subsection 5.2, this case leads to extra relativisitc degrees of freedom at BBN time so that $\Delta N_{\text{eff}}^{\text{BBN}} = 0.323$.

5.1 Thermal effect of hidden sectors on direct detection of dark matter

In this subsection we discuss the effect of a multi-hidden sector model on the determination of the relic density and on the spin-independent DM-proton cross section. The first observation to be made is regarding the effect of such a coupled system on the DM relic density. Here we consider case 1 but with $\kappa_1, \kappa_2 \sim 10^{-9}$ so that the contributions from ϕ_2 and ϕ_3 to the relic density are negligible. We solve the coupled Boltzmann equations for two cases: (A) $\xi_{i_0} = 1$ and (B) $\xi_{i_0} \ll 1$. We note that cases A and B result in different DM relic density such that $(\Omega h^2)_A < (\Omega h^2)_B$. The difference between the two can reach up to 50% in some cases, especially for $y_f \lesssim 10^{-8}$. To see why this is the case, one needs to examine the main annihilation process responsible for DM depletion. For $m_{\phi_1} \ll m_D$, the DM relic density is dominantly controlled by the annihilation process $D\bar{D} \to \phi_1\phi_1$ whose thermal average depends on the temperature T_1. In figure 7, we plot $n_D\langle\sigma v\rangle$ for $D\bar{D} \to \phi_1\phi_1$ versus the visible sector temperature for cases A and B. Also shown (in dashed line) is the Hubble parameter as well as the process $D\bar{D} \to i\,\bar{i}$ for comparison. The left panel of figure 7, which corresponds to a light mediator ($m_{\phi_1} = 1\,\text{MeV}$) and small y_f, shows that $D\bar{D} \to \phi_1\phi_1$ is far more dominant than $D\bar{D} \to i\bar{i}$ which can be explained by the relative sizes of the couplings y_f versus y_D. Furthermore, the rate of annihilation to $\phi_1\phi_1$ for case B (blue curve) overtakes the expansion rate earlier than for case A (red curve) and consequently decoupling also happens earlier. Thus for case A, the annihilation process continues for a longer time leading to a smaller relic density. This is in contrast to the case of a heavier mediator ($m_{\phi_1} = 1\,\text{GeV}$) and a larger y_f as shown in the right panel of figure 7 where one can see that $D\bar{D} \to \phi_1\phi_1$ decouples at the same instant for both cases A and B and thus the final yield is insensitive to whether the two sectors were initially at the same temperature or not.

To illustrate more concretely the effect of hidden sectors on observables in the visible sector, we use the latest constraints on the spin-independent (SI) DM-proton scattering

JHEP09(2022)084

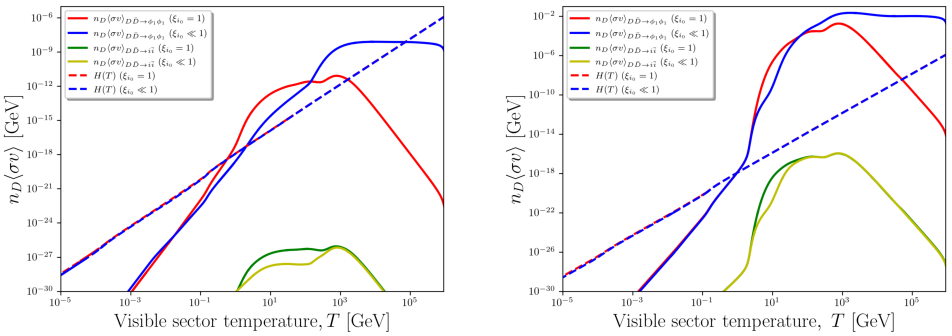

Figure 7. Display of $n_D\langle\sigma v\rangle$ for the processes $D\bar{D} \to \phi_1\phi_1$ and $D\bar{D} \to i\bar{i}$ versus T for two cases: $\xi_{i_0} = 1$ and $\xi_{i_0} \neq 1$. Input parameters for the left panel are: $m_D = 9.0\,\text{GeV}$, $m_{\phi_1} = 10\,\text{MeV}$, $m_{\phi_2} = m_{\phi_3} = 1\,\text{MeV}$, $y_f = 4.5 \times 10^{-10}$, $y_D = 0.13$ and $\kappa_1 = \kappa_2 = 5 \times 10^{-8}$. Input parameters for the right panel are: $m_D = 5.0\,\text{GeV}$, $m_{\phi_1} = 1\,\text{GeV}$, $m_{\phi_2} = m_{\phi_3} = 1\,\text{MeV}$, $y_f = 9.6 \times 10^{-6}$, $y_D = 0.18$ and $\kappa_1 = \kappa_2 = 1 \times 10^{-5}$.

cross-section from the PandaX-II collaboration. The collaboration presented their limits based on a secluded dark sector model of ref. [27] which considers a thermal DM distribution in the early universe. Using those limits, we recast the PandaX-II results to our model parameters and display the limits in the left panel of figure 8 (solid lines). The analysis which corresponds to the solid lines is for case A where we assume that the sectors have the same initial temperature. The dashed lines correspond to case B where the hidden sectors are initially much colder than the visible sector. We note that for 1 MeV and 10 MeV mediators the limits have moved up, i.e., have become more relaxed while for a 1 GeV mediator there is virtually no effect.

As discussed earlier, sectors at different temperatures lead to a larger relic density and so to reduce the value of the latter, one increases the coupling y_D which leads to a larger SI cross-section. Thus the limits move up as shown in the left panel of figure 8 (dashed lines). However, this seems not to be the case for a 1 GeV mediator. Also as discussed earlier, the main annihilation process decouples at the same time for cases A and B which results in no change in the relic density. This is due to the fact that in this case a larger y_f is required for those limits ($y_f \gtrsim 10^{-7}$) which takes us closer to a pure freeze-out case as the one used by PandaX-II to produce those limits. Thus as the coupling y_f increases, it gradually phases out the freeze-in mechanism [28] and we begin to agree with the limits presented in ref. [26]. This can be clearly seen in the right panel of figure 8 where the yield of D (red curve) reaches close to its equilibrium value (dashed brown curve) and then undergoes a freeze-out in a manner different from what appears for the cases of smaller y_f (see figures 2 and 4–6).

5.2 Dark radiation from hidden sectors

Hidden sectors in general contain extra relativistic degrees of freedom which will contribute to the so-called dark radiation which is constrained by BBN and CMB data. Thus, for example, for case 3, we have a massless spin zero field ϕ_3 which will remain in the spectrum

JHEP09(2022)084

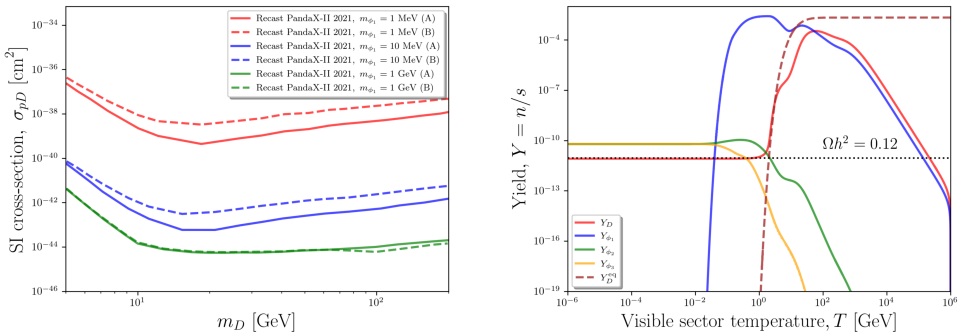

Figure 8. Left panel: a recast of the exclusion limits of the spin-independent proton-DM cross section, σ_{pD}, given by the PandaX-II Collaboration [26] for our model with two sets of initial hidden sector constraints, i.e., case A with $\xi_{i0} = 1$ (solid lines) and case B with $\xi_{i0} \ll 1$ (dashed lines) as a function of m_D for three different values of the pseudo-scalar ϕ_1 mass, i.e., m_{ϕ_1}=(1 MeV (red lines), 10 MeV (blue lines) and 1 GeV (green lines)). The coupling y_D for each point is chosen to give the correct DM relic density. Right panel: a plot of the yield of the dark particle species with the input: $m_D = 48$ GeV, $m_{\phi_1} = 1$ GeV, $m_{\phi_2} = m_{\phi_3} = 1$ MeV, $y_f = 10^{-7}$, $y_D = 0.55$ and $\kappa_1 = \kappa_2 = 1 \times 10^{-5}$.

and contribute to the relativistic degrees of freedom in the universe as dark radiation. Such a contribution over the existing neutrino species is determined by $\Delta N_{\rm eff}$, so that

$$\Delta N_{\rm eff} = \frac{8}{7}\left(\frac{11}{4}\right)^{4/3} \frac{\rho_{\rm DS}}{\rho_\gamma}, \tag{5.1}$$

where the energy density of the dark sector is $\rho_{\rm DS} = \rho_D(T_1) + \rho_{\phi_3}(T_3)$ and ρ_γ is the photon energy density. Based on the latest estimate of the effective number of neutrino species, $N_{\rm eff}$, from BBN [29]

$$N_{\rm eff} = 2.88 \pm 0.27, \tag{5.2}$$

where one can deduce a 2σ upper bound on $\Delta N_{\rm eff}$, so that $\Delta N_{\rm eff} < 0.42$. If ϕ_3 is produced efficiently and reaches an equilibrium distribution, then $\rho_{\phi_3} \propto T_3^4$ and from eq. (5.1) we have $\Delta N_{\rm eff} \sim (T_3/T)^4 = \xi_3^4$. So of particular importance to the determination of $\Delta N_{\rm eff}$ is the evolution of ξ_3 which is tightly coupled to the rest of the evolution parameters. In figure 6 we display the evolution of the yields and ξ_i for the case of a massless ϕ_3. For the set of assumed couplings, we have $\Delta N_{\rm eff}^{\rm BBN} = 0.323$ consistent with the BBN bound.

As noted, the constraint given in eq. (5.2) comes from BBN while other estimates of $N_{\rm eff}$ rely on the power spectrum data and CMB lensing from Planck and Baryon Acoustic Oscillations (BAO) [11, 30]. Further, local measurements of the Hubble parameter H_0 [31–33] show a significant deviation from estimates of H_0 at earlier times (see ref. [34] for a review of tensions in cosmology and ways to alleviate them and ref. [35] for a cosmologically consistent particle physics model aimed at alleviating the Hubble tension). A fit of the cosmological parameters to the CMB, BAO and local H_0 data points to a larger $\Delta N_{\rm eff}$ at the surface of last-scattering. The corresponding ranges for $\Delta N_{\rm eff}$ based on these analyses are shown in figure 9 as red and blue bands. The future CMB-S4 experiment [36, 37] is

JHEP09(2022)084

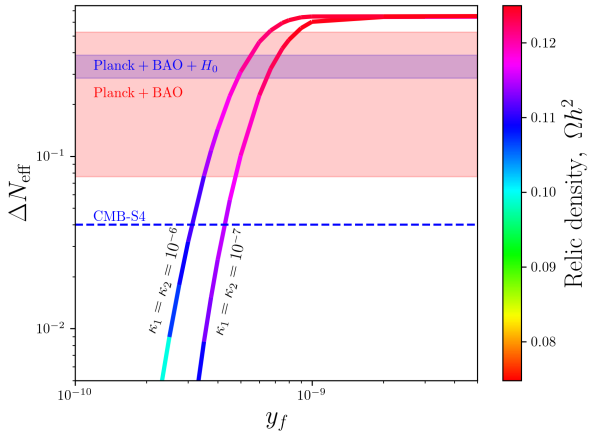

Figure 9. A plot of $\Delta N_{\rm eff}$ for the case of massless ϕ_3 as a function of y_f for sets of values of κ_1 and κ_2. The color gradient of the curves reflects the DM relic density. Other input parameters are same as in figure 6.

expected to reach a much better sensitivity in determining $N_{\rm eff}$ which will put stronger constraints on models predicting extra light relics. The projected sensitivity of CMB-S4 is shown as the dashed blue line in figure 9.

The curves in figure 9 show the variation in $\Delta N_{\rm eff}$ as a function of the coupling y_f for two sets of κ_1, κ_2. Since the hidden sectors form a chain with the visible sector then a change in y_f will eventually propagate to the third hidden sector thus affecting the energy density of ϕ_3 which is a function of the temperature T_3 (here enters the dependence on ξ_3). Larger y_f leads to larger contributions to $\Delta N_{\rm eff}$ until it saturates for $y_f \gtrsim 10^{-9}$ for the particular benchmark under consideration. Furthermore, larger values of κ_1 and κ_2 lead to a stronger coupling between the hidden sectors which eventually leads to an enhanced contribution to $\Delta N_{\rm eff}$ as evident when comparing the two curves in figure 9. The color gradient of the curves shows the change in the relic density as y_f varies. One can see that in the range of interest $\Omega h^2 \leq 0.12$. Based on our model, CMB-S4 can probe feeble couplings between the visible and hidden sectors down to $\mathcal{O}(10^{-10})$. Deviations from $N_{\rm eff}^{\rm SM}$ which are $\mathcal{O}(10^{-2})$ can point to relativistic relics that reside in hidden sectors at temperatures much lower than the visible sector temperature.

6 Conclusion

In a variety of supergravity, string and brane models one encounters hidden sectors which although neutral under the Standard Model gauge group can interact feebly with the visible sector via a variety of portals. In this work we have extended previous works where the visible sector was coupled to one or two hidden sectors to the case where an arbitrary number of hidden sectors are sequentially coupled to the visible sector. Thus the visible sector couples only to hidden sector 1 and the latter couples to hidden sector 2, and so on,

JHEP09(2022)084

i.e., in general the i-th hidden sector couples to hidden sectors $(i \pm 1)$. In general the visible and the hidden sectors will be in different heat baths, each with their own temperature. Of prime interest is to obtain the evolution equations for the ratio of temperatures in different heat baths after one has chosen a given temperature to serve as the clock. In the work here we use the temperature T of the visible sector as the clock and obtain the evolution equations for the ratios $T_i/T, i = 1, 2, \cdots, n$. A detailed analysis for the case of the visible sector coupled to three hidden sectors is given with an application to a simple model with scalar portals. We solve a set of coupled Boltzmann equations for particle yields and the temperature ratios ξ_i to trace the evolution of the dark species' population as well as the temperatures in each of the hidden sectors. We've shown that the presence of a chain of hidden sectors affects the DM relic density which comes out to be larger than one would get assuming all sectors are at the same temperature. A direct consequence of this observation is a modification of the recent PandaX-II limits on the SI DM-proton scattering cross sections for the case of self-interacting DM. Also we have seen that the hidden sectors thermalize with each other once the decay channels across the sectors are active. Further, assuming that one of the spin zero particles is massless, contributions to $\Delta N_{\rm eff}$ become an important constraint from cosmology. Weaker couplings between the different sectors lead to a smaller dark species' energy density and temperature ratios ξ_i. We expect the future CMB-S4 experiment to probe $\Delta N_{\rm eff}$ down to $\mathcal{O}(10^{-2})$ which would constraint our model in the very feeble coupling regime. We note that applications of the formalism developed here to other portals and to larger values of n beyond $n = 3$ and possibly to explore the region of large n should be of interest for future investigations. Finally, as noted in section 2, a chain of n hidden sectors appears in a broad class of beyond the Standard Model physics scenarios such as moose/quiver theories. Thus an analysis of the type discussed above may find application in this broad class of models.

Acknowledgments

The research of AA was supported by the BMBF under contract 05P21PMCAA and by the DFG through the Research Training Network 2149 "Strong and Weak Interactions — from Hadrons to Dark matter", while the research of PN was supported in part by the United States NSF Grant PHY-1913328 and PHY-2209903.

A Mass and temperature dependence of $g_{\rm eff}$ and $h_{\rm eff}$

The total effective number of energy density and entropy degrees of freedom in a sector containing a Dirac fermion and a boson are given by

$$g_{\rm eff} = g^b_{\rm eff} + \frac{7}{8} g^f_{\rm eff}, \quad \text{and} \quad h_{\rm eff} = h^b_{\rm eff} + \frac{7}{8} h^f_{\rm eff}, \tag{A.1}$$

JHEP09(2022)084

where the superscript b (f) indicates bosonic (fermionic) degrees of freedom where at temperature T, $g^b_{\rm eff}, h^b_{\rm eff}$ and $g^f_{\rm eff}, h^f_{\rm eff}$ are given by [38]

$$
\begin{aligned}
g^b_{\rm eff} &= \frac{15 d_b}{\pi^4}\int_{x_b}^{\infty}\frac{\sqrt{x^2-x_b^2}}{e^x-1}x^2dx, \quad \text{and} \quad h^b_{\rm eff} = \frac{15 d_b}{4\pi^4}\int_{x_b}^{\infty}\frac{\sqrt{x^2-x_b^2}}{e^x-1}\left(4x^2-x_b^2\right)dx, \\
g^f_{\rm eff} &= \frac{15 d_f}{\pi^4}\int_{x_f}^{\infty}\frac{\sqrt{x^2-x_f^2}}{e^x+1}x^2dx, \quad \text{and} \quad h^f_{\rm eff} = \frac{15 d_f}{4\pi^4}\int_{x_f}^{\infty}\frac{\sqrt{x^2-x_f^2}}{e^x+1}\left(4x^2-x_f^2\right)dx.
\end{aligned}
\tag{A.2}
$$

where d_b (d_f) are the intrinsic degrees of freedom for a bosonic (fermionic) field, so that for a massive spin 1, $d_b = 3$ and for a Dirac fermion $d_f = 4$. Further, x_b and x_f are defined so that $x_b = m_b/T$ and $x_f = m_f/T$. The limit $x_b \to 0$ gives $g^b_{\rm eff} = h^b_{\rm eff} \to d_b$ and the limit $x_f \to 0$ gives $g^f_{\rm eff} = h^f_{\rm eff} \to d_f$.

B Collision and source terms

In this appendix we list the collision terms appearing in eq. (4.20) and the source terms appearing in eqs. (4.17)–(4.19) for particles D, ϕ_1, ϕ_2 and ϕ_3. The respective collision terms are given by

$$
\begin{aligned}
&\mathcal{Q}_D = \\
&\tfrac{1}{2}\langle\sigma v\rangle_{D\bar{D}\to f\bar{f}}(T)\left(Y_D^{\rm eq}(T)^2 - Y_D^2\right) - \tfrac{1}{2}\langle\sigma v\rangle_{D\bar{D}\to\phi_1\phi_1}(T_1)\left(Y_D^2 - Y_D^{\rm eq}(T_1)^2\frac{Y_{\phi_1}^2}{Y_{\phi_1}^{\rm eq}(T_1)^2}\right),
\end{aligned}
\tag{B.1}
$$

$$
\begin{aligned}
&\mathcal{Q}_{\phi_1} = \\
&\langle\sigma v\rangle_{\phi_1\phi_1\to f\bar{f}}(T)(Y_{\phi_1}^{\rm eq}(T)^2 - Y_{\phi_1}^2) + \tfrac{1}{2}\langle\sigma v\rangle_{D\bar{D}\to\phi_1\phi_1}(T_1)\left(Y_D^2 - Y_D^{\rm eq}(T_1)^2\frac{Y_{\phi_1}^2}{Y_{\phi_1}^{\rm eq}(T_1)^2}\right) \\
&+\langle\sigma v\rangle_{f\bar{f}\to\phi_1}(T)\left(Y_q^{\rm eq}(T)^2 - Y_q^{\rm eq}(T)^2\frac{Y_{\phi_1}}{Y_{\phi_1}^{\rm eq}(T_1)}\right) - \langle\sigma v\rangle_{\phi_1\phi_1\to\phi_2\phi_2}(T_1)\left(Y_{\phi_1}^2 - Y_{\phi_1}^{\rm eq}(T_1)^2\frac{Y_{\phi_2}^2}{Y_{\phi_2}^{\rm eq}(T_2)^2}\right) \\
&+\langle\sigma v\rangle_{\phi_3\phi_3\to\phi_1\phi_1}(T_3)\left(Y_{\phi_3}^2 - Y_{\phi_3}^{\rm eq}(T_3)^2\frac{Y_{\phi_1}^2}{Y_{\phi_1}^{\rm eq}(T_1)^2}\right) - \langle\sigma v\rangle_{\phi_1\phi_1\to\phi_2}(T_1)\left(Y_{\phi_1}^2 - Y_{\phi_1}^{\rm eq}(T_1)^2\frac{Y_{\phi_2}}{Y_{\phi_2}^{\rm eq}(T_2)}\right),
\end{aligned}
\tag{B.2}
$$

$$
\begin{aligned}
&\mathcal{Q}_{\phi_2} = \\
&\langle\sigma v\rangle_{\phi_1\phi_1\to\phi_2\phi_2}(T_1)\left(Y_{\phi_1}^2 - Y_{\phi_1}^{\rm eq}(T_1)^2\frac{Y_{\phi_2}^2}{Y_{\phi_2}^{\rm eq}(T_2)^2}\right) + \langle\sigma v\rangle_{\phi_1\phi_1\to\phi_2}(T_1)\left(Y_{\phi_1}^2 - Y_{\phi_1}^{\rm eq}(T_1)^2\frac{Y_{\phi_2}}{Y_{\phi_2}^{\rm eq}(T_2)}\right) \\
&+\langle\sigma v\rangle_{\phi_3\phi_3\to\phi_2\phi_2}(T_3)\left(Y_{\phi_3}^2 - Y_{\phi_3}^{\rm eq}(T_3)^2\frac{Y_{\phi_2}^2}{Y_{\phi_2}^{\rm eq}(T_2)^2}\right) + \langle\sigma v\rangle_{\phi_3\phi_3\to\phi_2}(T_3)\left(Y_{\phi_3}^2 - Y_{\phi_3}^{\rm eq}(T_3)^2\frac{Y_{\phi_2}}{Y_{\phi_2}^{\rm eq}(T_2)}\right),
\end{aligned}
\tag{B.3}
$$

$$
\begin{aligned}
&\mathcal{Q}_{\phi_3} = \\
&-\langle\sigma v\rangle_{\phi_3\phi_3\to\phi_2\phi_2}(T_3)\left(Y_{\phi_3}^2 - Y_{\phi_3}^{\rm eq}(T_3)^2\frac{Y_{\phi_2}^2}{Y_{\phi_2}^{\rm eq}(T_2)^2}\right) - \langle\sigma v\rangle_{\phi_3\phi_3\to\phi_1\phi_1}(T_3)\left(Y_{\phi_3}^2 - Y_{\phi_3}^{\rm eq}(T_3)^2\frac{Y_{\phi_1}^2}{Y_{\phi_1}^{\rm eq}(T_1)^2}\right) \\
&-\langle\sigma v\rangle_{\phi_3\phi_3\to\phi_2}(T_3)\left(Y_{\phi_3}^2 - Y_{\phi_3}^{\rm eq}(T_3)^2\frac{Y_{\phi_2}}{Y_{\phi_2}^{\rm eq}(T_2)}\right)\Bigg].
\end{aligned}
\tag{B.4}
$$

JHEP09(2022)084

The source terms are given by

$$
\begin{aligned}
j_1 = & \\
& 2n_f^{\rm eq}(T)^2\left(1-\frac{n_D^2}{n_D^{\rm eq}(T_1)^2}\right)J(f\bar{f}\to D\bar{D}) + 2n_q^{\rm eq}(T)^2\left(1-\frac{n_{\phi_1}^2}{n_{\phi_1}^{\rm eq}(T_1)^2}\right)J(f\bar{f}\to\phi_1\phi_1) \\
& + n_q^{\rm eq}(T)^2 J(f\bar{f}\to\phi_1) - n_{\phi_1}J(\phi_1\to f\bar{f}) + 2\left(n_{\phi_2}-n_{\phi_2}^{\rm eq}\frac{n_{\phi_1}^2}{n_{\phi_1}^{\rm eq}(T_1)^2}\right)J(\phi_2\to\phi_1\phi_1) \\
& - 2\left(n_{\phi_1}^2-n_{\phi_1}^{\rm eq}(T_1)^2\frac{n_{\phi_2}^2}{n_{\phi_2}^{\rm eq}(T_2)^2}\right)J(\phi_1\phi_1\to\phi_2\phi_2) \\
& - 2\left(n_{\phi_1}^2-n_{\phi_1}^{\rm eq}(T_1)^2\frac{n_{\phi_3}^2}{n_{\phi_3}^{\rm eq}(T_3)^2}\right)J(\phi_1\phi_1\to\phi_3\phi_3),
\end{aligned}
\tag{B.5}
$$

$$
\begin{aligned}
j_2 = & \\
& -\left(n_{\phi_2}-n_{\phi_2}^{\rm eq}\frac{n_{\phi_1}^2}{n_{\phi_1}^{\rm eq}(T_1)^2}\right)J(\phi_2\to\phi_1\phi_1) + 2\left(n_{\phi_1}^2-n_{\phi_1}^{\rm eq}(T_1)^2\frac{n_{\phi_2}^2}{n_{\phi_2}^{\rm eq}(T_2)^2}\right)J(\phi_1\phi_1\to\phi_2\phi_2) \\
& + 2\left(n_{\phi_3}^2-n_{\phi_3}^{\rm eq}(T_3)^2\frac{n_{\phi_2}^2}{n_{\phi_2}^{\rm eq}(T_2)^2}\right)J(\phi_3\phi_3\to\phi_2\phi_2) - \left(n_{\phi_2}-n_{\phi_2}^{\rm eq}\frac{n_{\phi_3}^2}{n_{\phi_3}^{\rm eq}(T_3)^2}\right)J(\phi_2\to\phi_3\phi_3),
\end{aligned}
\tag{B.6}
$$

$$
\begin{aligned}
j_3 = & \\
& -2\left(n_{\phi_3}^2-n_{\phi_3}^{\rm eq}(T_3)^2\frac{n_{\phi_2}^2}{n_{\phi_2}^{\rm eq}(T_2)^2}\right)J(\phi_3\phi_3\to\phi_2\phi_2) + 2\left(n_{\phi_2}-n_{\phi_2}^{\rm eq}\frac{n_{\phi_3}^2}{n_{\phi_3}^{\rm eq}(T_3)^2}\right)J(\phi_2\to\phi_3\phi_3) \\
& + 2\left(n_{\phi_1}^2-n_{\phi_1}^{\rm eq}(T_1)^2\frac{n_{\phi_3}^2}{n_{\phi_3}^{\rm eq}(T_3)^2}\right)J(\phi_1\phi_1\to\phi_3\phi_3).
\end{aligned}
\tag{B.7}
$$

In the above we have

$$
n_f^{\rm eq}(T)^2 J\left(f\bar{f}\to XX\right)(T) = \frac{T}{32\pi^4}\int_{4m_D^2}^{\infty} ds\ \sigma_{XX\to f\bar{f}}s(s-s_0)K_2\left(\sqrt{s}/T\right), \tag{B.8}
$$

$$
n_q^{\rm eq}(T)^2 J\left(f\bar{f}\to\phi_1\right)(T) = \frac{T}{32\pi^4}\int_{s_0}^{\infty} ds\ \sigma_{f\bar{f}\to\phi_1}s(s-s_0)K_2(\sqrt{s}/T), \tag{B.9}
$$

$$
n_X(T_i)^2 J(XX\to YY)(T_i) = \frac{n_X(T_i)^2}{8m_X^4 T_i K_2^2(m_X/T_i)}\int_{s_0}^{\infty} ds\ \sigma_{XX\to YY}s(s-s_0)K_2(\sqrt{s}/T_i), \tag{B.10}
$$

$$
n_X J(X\to YY)(T_i) = n_X m_X \Gamma_{X\to YY}\,. \tag{B.11}
$$

JHEP09(2022)084

References

[1] L. Ackerman, M.R. Buckley, S.M. Carroll and M. Kamionkowski, *Dark Matter and Dark Radiation*, *Phys. Rev. D* **79** (2009) 023519 [arXiv:0810.5126] [INSPIRE].

[2] L. Heurtier, Y. Mambrini and M. Pierre, *Dark matter interpretation of the ANITA anomalous events*, *Phys. Rev. D* **99** (2019) 095014 [arXiv:1902.04584] [INSPIRE].

[3] A. Aboubrahim, W.-Z. Feng, P. Nath and Z.-Y. Wang, *Self-interacting hidden sector dark matter, small scale galaxy structure anomalies, and a dark force*, *Phys. Rev. D* **103** (2021) 075014 [arXiv:2008.00529] [INSPIRE].

[4] A. Aboubrahim, W.-Z. Feng, P. Nath and Z.-Y. Wang, *A multi-temperature universe can allow a sub-MeV dark photon dark matter*, *JHEP* **06** (2021) 086 [arXiv:2103.15769] [INSPIRE].

[5] J.D. Bowman, A.E.E. Rogers, R.A. Monsalve, T.J. Mozdzen and N. Mahesh, *An absorption profile centred at* 78 *megahertz in the sky-averaged spectrum*, *Nature* **555** (2018) 67 [arXiv:1810.05912] [INSPIRE].

[6] A. Aboubrahim, P. Nath and Z.-Y. Wang, *A cosmologically consistent millicharged dark matter solution to the EDGES anomaly of possible string theory origin*, *JHEP* **12** (2021) 148 [arXiv:2108.05819] [INSPIRE].

[7] J.B. Muñoz and A. Loeb, *A small amount of mini-charged dark matter could cool the baryons in the early Universe*, *Nature* **557** (2018) 684 [arXiv:1802.10094] [INSPIRE].

[8] J.B. Muñoz, C. Dvorkin and A. Loeb, 21*-cm Fluctuations from Charged Dark Matter*, *Phys. Rev. Lett.* **121** (2018) 121301 [arXiv:1804.01092] [INSPIRE].

[9] H. Liu, N.J. Outmezguine, D. Redigolo and T. Volansky, *Reviving Millicharged Dark Matter for 21-cm Cosmology*, *Phys. Rev. D* **100** (2019) 123011 [arXiv:1908.06986] [INSPIRE].

[10] A. Berlin, D. Hooper, G. Krnjaic and S.D. McDermott, *Severely Constraining Dark Matter Interpretations of the 21-cm Anomaly*, *Phys. Rev. Lett.* **121** (2018) 011102 [arXiv:1803.02804] [INSPIRE].

[11] Planck collaboration, *Planck 2018 results. VI. Cosmological parameters*, *Astron. Astrophys.* **641** (2020) A6 [*Erratum ibid.* **652** (2021) C4] [arXiv:1807.06209] [INSPIRE].

[12] R. Foot and S. Vagnozzi, *Dissipative hidden sector dark matter*, *Phys. Rev. D* **91** (2015) 023512 [arXiv:1409.7174] [INSPIRE].

[13] R. Foot and S. Vagnozzi, *Solving the small-scale structure puzzles with dissipative dark matter*, *JCAP* **07** (2016) 013 [arXiv:1602.02467] [INSPIRE].

[14] I. Rothstein and W. Skiba, *Mother Moose: generating extra dimensions from simple groups at large N*, *Phys. Rev. D* **65** (2002) 065002 [hep-th/0109175] [INSPIRE].

[15] M.R. Douglas and G.W. Moore, *D-branes, quivers, and ALE instantons*, hep-th/9603167 [INSPIRE].

[16] N. Arkani-Hamed, A.G. Cohen and H. Georgi, *(De)constructing dimensions*, *Phys. Rev. Lett.* **86** (2001) 4757 [hep-th/0104005] [INSPIRE].

[17] C.T. Hill, S. Pokorski and J. Wang, *Gauge Invariant Effective Lagrangian for Kaluza-Klein Modes*, *Phys. Rev. D* **64** (2001) 105005 [hep-th/0104035] [INSPIRE].

[18] A. Aboubrahim, W.-Z. Feng, P. Nath and Z.-Y. Wang, *Hidden sectors and a multi-temperature universe*, in *2022 Snowmass Summer Study*, Washington University, Seattle, U.S.A., July 17–26 2022 [arXiv:2106.06494] [INSPIRE].

[19] B. Holdom, *Two* U(1)*'s and Epsilon Charge Shifts*, *Phys. Lett. B* **166** (1986) 196 [INSPIRE].

JHEP09(2022)084

[20] B. Körs and P. Nath, *A Stueckelberg extension of the standard model*, *Phys. Lett. B* **586** (2004) 366 [hep-ph/0402047] [INSPIRE].

[21] D. Feldman, Z. Liu and P. Nath, *The Stueckelberg Z-prime Extension with Kinetic Mixing and Milli-Charged Dark Matter From the Hidden Sector*, *Phys. Rev. D* **75** (2007) 115001 [hep-ph/0702123] [INSPIRE].

[22] K. Cheung and T.-C. Yuan, *Hidden fermion as milli-charged dark matter in Stueckelberg Z′ model*, *JHEP* **03** (2007) 120 [hep-ph/0701107] [INSPIRE].

[23] A. Aboubrahim, W.-Z. Feng and P. Nath, *A long-lived stop with freeze-in and freeze-out dark matter in the hidden sector*, *JHEP* **02** (2020) 118 [arXiv:1910.14092] [INSPIRE].

[24] M. Du, Z. Liu and P. Nath, *CDF W mass anomaly from a dark sector with a Stueckelberg-Higgs portal*, arXiv:2204.09024 [INSPIRE].

[25] A. Aboubrahim, T. Ibrahim, M. Klasen and P. Nath, *A decaying neutralino as dark matter and its gamma ray spectrum*, *Eur. Phys. J. C* **81** (2021) 680 [arXiv:2012.10795] [INSPIRE].

[26] PandaX-II collaboration, *Constraining self-interacting dark matter with the full dataset of PandaX-II*, *Sci. China Phys. Mech. Astron.* **64** (2021) 111062 [arXiv:2104.14724] [INSPIRE].

[27] R. Huo, M. Kaplinghat, Z. Pan and H.-B. Yu, *Signatures of Self-Interacting Dark Matter in the Matter Power Spectrum and the CMB*, *Phys. Lett. B* **783** (2018) 76 [arXiv:1709.09717] [INSPIRE].

[28] L.J. Hall, K. Jedamzik, J. March-Russell and S.M. West, *Freeze-In Production of FIMP Dark Matter*, *JHEP* **03** (2010) 080 [arXiv:0911.1120] [INSPIRE].

[29] C. Pitrou, A. Coc, J.-P. Uzan and E. Vangioni, *Precision big bang nucleosynthesis with improved Helium-4 predictions*, *Phys. Rept.* **754** (2018) 1 [arXiv:1801.08023] [INSPIRE].

[30] Planck collaboration, *Planck 2018 results. I. Overview and the cosmological legacy of Planck*, *Astron. Astrophys.* **641** (2020) A1 [arXiv:1807.06205] [INSPIRE].

[31] A.G. Riess et al., *A Comprehensive Measurement of the Local Value of the Hubble Constant with 1 KM s^{-1} Mpc^{-1} Uncertainty from the Hubble Space Telescope and the SH0ES Team*, *Astrophys. J. Lett.* **934** (2022) L7 [arXiv:2112.04510] [INSPIRE].

[32] A.G. Riess et al., *New Parallaxes of Galactic Cepheids from Spatially Scanning the Hubble Space Telescope: Implications for the Hubble Constant*, *Astrophys. J.* **855** (2018) 136 [arXiv:1801.01120] [INSPIRE].

[33] A.G. Riess, S. Casertano, W. Yuan, L.M. Macri and D. Scolnic, *Large Magellanic Cloud Cepheid Standards Provide a 1% Foundation for the Determination of the Hubble Constant and Stronger Evidence for Physics beyond ΛCDM*, *Astrophys. J.* **876** (2019) 85 [arXiv:1903.07603] [INSPIRE].

[34] E. Abdalla et al., *Cosmology intertwined: A review of the particle physics, astrophysics, and cosmology associated with the cosmological tensions and anomalies*, *JHEAp* **34** (2022) 49 [arXiv:2203.06142] [INSPIRE].

[35] A. Aboubrahim, M. Klasen and P. Nath, *Analyzing the Hubble tension through hidden sector dynamics in the early universe*, *JCAP* **04** (2022) 042 [arXiv:2202.04453] [INSPIRE].

[36] CMB-S4 collaboration, *CMB-S4 Science Book, First Edition*, arXiv:1610.02743 [INSPIRE].

[37] CMB-S4 collaboration, *Snowmass 2021 CMB-S4 White Paper*, arXiv:2203.08024 [INSPIRE].

[38] M. Hindmarsh and O. Philipsen, *WIMP dark matter and the QCD equation of state*, *Phys. Rev. D* **71** (2005) 087302 [hep-ph/0501232] [INSPIRE].

JHEP09(2022)084